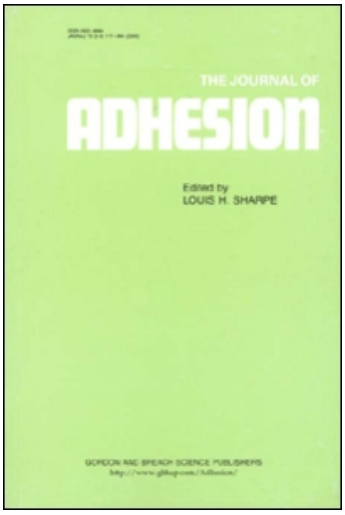

The Journal of Adhesion
Publication details, including instructions for authors and subscription information:
http://www.informaworld.com/smpp/title~content=t713453635

A Finite Element Analysis of Cracks in the Region of a Bi-Material Interface

Charless W. Fowlkes[a]
[a] Engineering Mechanics Dept., Vanderbilt University, Nashville, Tennessee, U.S.A.

To cite this Article Fowlkes, Charless W.(1974) 'A Finite Element Analysis of Cracks in the Region of a Bi-Material Interface', The Journal of Adhesion, 6: 1, 49 — 84
To link to this Article: DOI: 10.1080/00218467408072238
URL: http://dx.doi.org/10.1080/00218467408072238

J. Adhesion, 1974, Vol. 6, pp. 49–84

Printed in Northern Ireland

A Finite Element Analysis of Cracks in the Region of a Bi-Material Interface†

CHARLESS W. FOWLKES‡

Engineering Mechanics Dept., Vanderbilt University, Nashville, Tennessee, U.S.A.

(*Received December 15, 1972*)

This work was motivated by the fact that the fracture toughness of composite materials is strongly related to the micromechanics of the fracture process. The effects of interfacial bonding, interfacial splitting, fiber pull-out, matrix cracking, fiber failure, etc. on the gross composite strength and toughness have been widely discussed in the literature. This work considers simplified analytical models of some of these mechanisms which permits quantitative evaluations of the roles of material properties as related to microfracture mechanisms.

A micro-model of the interfacial region in a two-phase composite is analyzed. The model is a rectangular region loaded at the boundaries. The region is divided into Phase I and Phase II by a vertical line representing the interface. Several crack geometries are modeled including a crack in Phase I approaching the interface and extending to the interface, a crack extending along the interface and a crack penetrating the interface and extending into Phase II.

These models are analyzed by the finite element method incorporating a special crack-tip element. The concepts of linear elastic fracture mechanics were incorporated into the analysis and the fracture parameters G and K were determined for each of the crack geometries for a range of modulus ratios. These results are used to discuss the tendencies toward the various modes of crack progression as functions of the material and interfacial properties.

INTRODUCTION

The continuum approach of characterizing static and fatigue strength of homogeneous materials can be transferred directly to composite materials

† Presented at the Symposium on "Interfacial Bonding and Fracture in Polymeric, Metallic and Ceramic Composites" at The Univ. of California at Los Angeles, Nov. 13–15, 1972. This Symposium was jointly sponsored by the Polymer Group of So. California Section, ACS and Materials Science Department, U.C.L.A.

‡ Present address: Cryogenics Division, Institute for Basic Standards, National Bureau of Standards, Boulder, Colorado 80302, U.S.A.

although it is usually necessary to account for anisotropy with additional parameters.[1] Fracture theories for homogeneous materials are all centered around some model of the crack tip region. The output of these theories is a relationship between the strength of the part and the size of the crack. Since parts made of homogeneous materials usually fail due to the propagation of a single crack from the largest flaw, these "one crack" theories have direct application.

While the crack in a homogeneous material is generally a single well defined discontinuity, and the fracture surface is relatively smooth, the fracture of a composite is generally accompanied by the formation and growth of multiple microcracks which are distributed over large regions in the material. Some of these microcracks eventually join to create a discontinuity through the part. The fracture mechanics concepts developed for homogeneous materials cannot be expected to apply in general to composite materials due to the fact that composite materials usually do not fail due to the propagation of a single crack. Two modes of composite fracture to which fracture mechanics could be applied are represented in the schematic drawings in Figure 1(a).[2] The mode of fracture represented in Figure 1(b) might be adequately described by fracture mechanics if the *splitting* was always

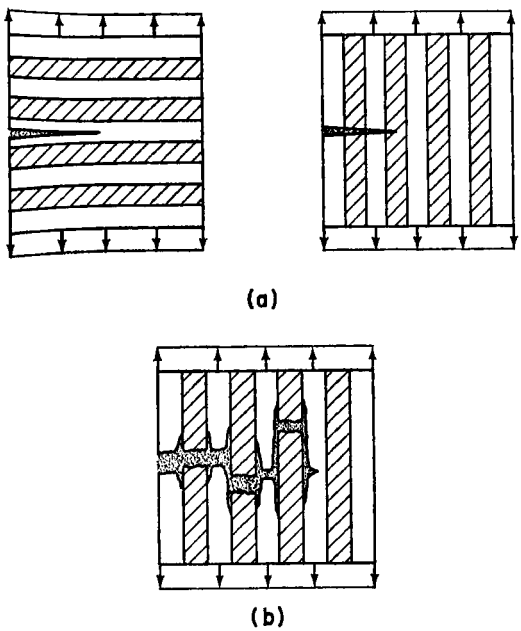

FIGURE 1a Composite fracture modes in which there is a single, well defined crack.
FIGURE 1b Composite fracture mode which exhibits splitting.

limited to some small region near the "crack" tip and was independent of "crack" length.[3,4]

Microfracture mechanics

By suitably reducing the frame of reference to the microscale, it is possible to arrive at a point at which the frame of reference includes only one crack. This procedure is schematically represented in Figure 2. At the microfracture level, since there is only a single crack, it is possible to apply the concepts of fracture mechanics, and to characterize the tendency for the crack to propagate. In Figure 2, several basic modes of microfracture are identified.[5,6,7,8,9,10,11,12,13,14]

The high fracture toughness of composites is in general due to the fact that the reinforcement (or the matrix) will act as crack arrestors. The microfracture event associated with this mechanism is the case of a crack intercepting an interface. The toughness of the bulk composite material will normally be increased if the crack is arrested at the interface and subsequently *splits* and propagates along the interface. Splitting is schematically represented in Figure 1(b).

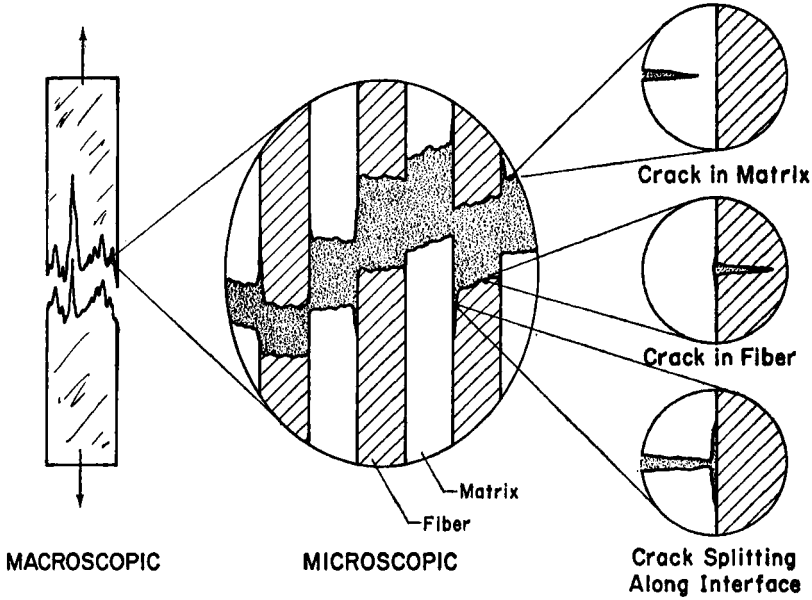

FIGURE 2 Some basic microfracture modes.

In this paper several micromechanical fracture modes which relate to the splitting of the crack as it intercepts a bi-material interface are analyzed. Finite element fracture analyses are performed and the implications of the results to composite fracture are discussed.

Fracture mechanics

Fracture mechanics deals with crack propagation phenomena and is concerned with the stability of pre-existing flaws. This technology has produced specific parameters which serve to characterize the resistance to crack propagation or fracture toughness of homogeneous materials. Two common parameters used in linear elastic fracture mechanics are G and K. G is based on energy considerations and for a cracked body having a crack of length a

$$G = -\frac{\partial U}{\partial a} \tag{1}$$

where U is the internal energy of the body. This parameter was first proposed by Griffith[15] in the course of his experiments on the fracture of glass and later extended to other structural materials by Irwin[16]. K for a cracked body is of the general form

$$K = C\sigma\sqrt{a} \tag{2}$$

where σ is applied stress, a is the crack length and C depends on the geometry of the body. For a particular structure containing a crack and subjected to some load, G is termed "the crack extension force" and K is termed "the stress intensity factor".

For a particular material there are critical values of G and K which correspond to the onset of crack propagation. These quantities are symbolized by G_c and K_c where G_c is termed "the fracture toughness" and K_c is termed "the critical stress intensity factor".

For problems of in plane loading the two modes of crack surface displacement are classified as opening mode (I) and sliding mode (II). A drawing illustrating these modes of displacement is shown in Figure 3. Separate stress intensity factors (K) and strain energy release rates (G) are identified with the two modes of crack displacement by attaching the subscripts I and II. The stress intensity factor for a structure containing a crack and loaded so as to cause crack displacement of type I opening mode is denoted as K_I. If the crack is subjected to more than one mode of displacement the situation is referred to as "mixed mode". The stresses and displacements for mixed mode are combined by superposition.

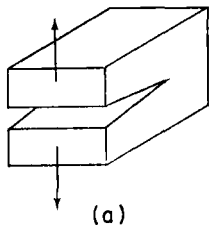

FIGURE 3a Opening displacement, Mode I.

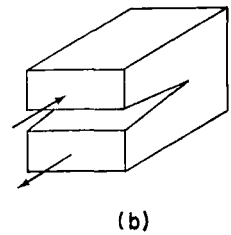

FIGURE 3b Sliding displacement, Mode II.

The relationship between G_I and K_I for plane strain is given by Irwin[17] as

$$K_I = \left[\frac{G_I E}{(1-\nu^2)}\right]^{1/2} \tag{3}$$

where E is Young's modulus and ν is Poisson's ratio.

Fracture mechanics thus provides a design procedure which can be used to predict crack extension. The first step is to determine the constant C and hence K_I in (2) which depends on the geometry and type of loading. The next step is to determine K_{Ic} for the material using a suitable laboratory fracture toughness specimen. Setting $K_I = K_{Ic}$ in (2) results in critical combinations of stress and crack length. Thus for a given flaw size or crack length determined by inspection of the structure, the load causing crack extension is known from (2).

Cracks parallel to a bi-material interface

Several investigators have worked on analytical solutions for the stress fields in the region of a crack on a bi-material interface. Muskhelishvili[18] presented an elasticity solution to the problem of a stamp of one material of finite width pressed onto a semi-finite half plane of a second material. Although this was not a crack problem, the method of solution which used the eigenfunction expansion approach was later used for the solution of crack problems.

Williams[19] considered the plane problem of dissimilar materials with a semi-infinite crack along the bi-material interface. Near the crack tip the stresses were found to follow the $\sqrt{r}$ singularity as in homogeneous materials where r is a polar coordinate about the crack tip. The eigenfunction-expansion approach was used and the solution predicted oscillating stresses in the region of the crack tip. Erdogan[20] considered the problem of two semi-infinite elastic planes with different elastic properties bonded to each other

along a finite number of straight-line segments and subjected to loads at infinity. Using an analysis procedure similar to the above, Erdogan's results likewise predict a $\sqrt{r}$ singularity and oscillating stresses near the crack tip. Erdogan carries the problem further by defining a stress intensity factor for this geometry.

Rice and Sih[21,22] expanded Williams' work on a model consisting of a semi-infinite crack lying along a bi-material interface with concentrated forces acting on a crack face. They carried their results to the determination of the stress intensity factors.

Sih[23,24] has presented solutions for several multiple-layer models containing cracks along the interfaces and cracks in the sandwiched layer parallel to the interfaces. For the cases of interfacial cracks the characteristic singularity is the same as in the previously reported problems. It might be noted that for some cases of an interlaminar crack the nature of the singularity departs from $\sqrt{r}$ as the thickness of the layer containing the crack becomes small. Sih also suggests that since the oscillating characteristic of the stresses has never been observed experimentally the models used for these analyses may not be entirely valid. In Ref. 23 the relationship of these results to composite microfracture is discussed.

A limiting case of a crack in a sandwiched bi-material model is the case of the fracture of an adhesive joint. References 7 and 25 explore the application of the concepts of linear elastic fracture mechanics to the fracture of adhesive joints. These experiments were interpreted from a Griffith energy viewpoint and this resulted in a meaningful fracture criteria.

Tensile tests of butt-joined epoxy aluminum plates containing single cracks along the bond surfaces have been reported in Ref. 26. The results were compared to the theories presented by Erdogan and Sih and Rice and agreed reasonably well for a specified range of crack lengths.

Cracks perpendicular to a bi-material interface

Zak and Williams,[27] as a continuation of Williams' analysis of a crack lying along an interface, presented a solution for the stress field in the region of a crack perpendicular to a bi-material interface with the crack tip on the interface. They established equations for the stresses in terms of eigenfunctions and one undetermined constant and evaluated the effect of the elastic moduli on the form of the stress singularity. As with the previous eigenfunction solutions, oscillating stresses result at the crack tip. In contrast to the solution for a crack in a homogeneous material or parallel to and on a bi-material interface, they found that the characteristic singularity varied as $r^{\lambda+1}$ where

λ is an eigenparameter and depends on the material properties. They did not report the magnitudes of the stress components in the region.

In a later paper, Swenson and Rau[28] extended the analysis of Williams and Zak. They solved for the relative stresses for plane stress and plane strain to within an arbitrary constant for an unspecified case of symmetrical plane loading. They presented results for the relative near-tip stress components at points ahead of the crack tip and along the interface located at an arbitrary radius. These stress ratios were determined for a wide range of moduli and the implications of the results to composite fracture were discussed. No attempts were made to relate these results to the concepts of fracture mechanics.

A recent paper by Leverenz[29] reports the results of a finite element analysis of a cracked bi-material plate where the crack is oriented normal to but not touching the bi-material interface. Since the crack tip was totally contained in one of the homogeneous materials and was some distance from the interface a square root singularity was assumed. The author presents values for K_I for a range of moduli and crack lengths.

The theory of linear elastic fracture mechanics is based on the $\sqrt{r}$ singularity. Experience has shown this concept to be operationally valid for predicting critical conditions in some types of problems. Problems having some different type of singularity may require the evolution of another fracture theory. This is the situation which arises in the case of cracks near a bi-material interface.

Finite element fracture analysis

Analytical solutions for the fracture parameters G_I or K_I are available for several simple geometries and loading conditions. For finite structures, complicated loading and irregular cracks, approximate methods must be used to determine the stress intensity factors. The finite element method has recently been applied as an analytical tool to fracture problems.

The finite element method approximates the continuum as a finite assemblage of finite elements. These elements are interconnected at a finite number of nodal points and are subjected to some of the constraints that exist in a continuum. Internal forces are transmitted through the interior nodes. Finite element analysis is widely used and the procedures are well documented in numerous papers and books.[30] The constant strain triangular elements (CST) were used in this paper except where noted otherwise.

The earliest papers concerning the application of finite element analysis toward the determination of G_I and K_I appeared a few years ago. Since then

a large number of papers have been published proposing a variety of approaches to the problem. A recent survey of these approaches is contained in Ref. 31. The approaches can be generally classified as energy methods and direct (stress or displacement) methods and are outlined below.

Total energy method

The total energy approach is based on the definition of G given in (1). Using this method a finite element idealization of the body containing the crack is constructed. This problem is solved and the total internal energy is determined by either computing the external work or by summing the element strain energy. The crack length is then changed by a small amount Δa and the problem is solved again and the new strain energy determined. The quantity $\Delta U/\Delta a$ can be determined from the two solutions and is a numerical approximation of $\partial U/\partial a$ as defined in (1).[32,33]

Local energy methods

Irwin[17] gives an expression for the crack extension force in terms of the strain energy density in a circular region surrounding the crack tip. This method of calculating the stress intensity factor has not been extensively used due to the necessity of defining a circular region in the finite element net.[31]

Another local energy method is referred to as the J-integral method. J is defined in terms of a line integral along an arbitrary contour enclosing the crack tip.[34] The J-integral has been used for finite element fracture analysis by several investigators.[29,32,35,36]

Direct methods

The direct methods are based on the well known crack tip equations.[17] A finite element solution will yield approximate values of stress and displacements at discreet points in the body. At points near the crack tip, values of stress or displacement from the finite element solution may be substituted into the crack tip equations and these equations solved for K_I.

Since displacements are the fundamental quantities determined from the finite element solution, values K_I determined from the crack tip displacement equations are more reliable.[31,32,35,37]

Displacement method

Most investigators also agree that K_I is most accurately determined by using the nodal displacements along the free surface of the crack. The stresses in the crack tip region vary as $1/\sqrt{r}$, leading to steep gradients and a singularity in stress at the crack tip ($r = 0$). If constant strain elements (CST) are used a very large number of elements must be placed in the near-tip region in order to model these steep gradients.[32,35,36,37] Comparisons of finite element solutions with known solutions show that K_I can be determined to within 4 percent using (approximately) 500 CST elements.[32,35] If the total number of elements is increased and the mesh near the crack tip is dense and distributed as $\sqrt{r}$, K_I may be determined to within nearly 1 percent.[32]

The displacement of the node nearest the crack tip can be used but an improvement in the value of K_I can be obtained if several values of displacement along the crack face near the tip are used and the resulting curve extrapolated back to $r = 0$ and the intercept taken as the value of K_I. It has been shown that this procedure results in the best estimate of K_I for a finite element fracture solution.[31,35]

Crack tip element

In order to reduce the number of elements required and the subsequent cost of finite element fracture analysis several investigators have devised special crack tip elements.[37,38,39,40,41,42] Although the formulations of the various elements are different they share the common feature of having displacement functions of the form of the crack tip displacement equations. It has been demonstrated that if the dense net of CST elements surrounding the crack tip is replaced by a single[38] or several[37,39,42] special crack tip singularity elements the computation time is reduced and the accuracy is improved.

A crack tip element developed by Wilson[37] was used for the problems considered in this report. This element is triangular in shape and has a displacement function which approximates the $\sqrt{r}$ singularity. This element is referred to as the SST element and a detailed discussion is given in Ref. 37.

For the problems analyzed in this paper, 12 SST elements were used having a radius of approximately 10 percent of the crack length. The models had from 130 to 185 nodes. The stress intensity factors were computed from the displacement of the first node. In some cases it was possible to use the extrapolation method and for these cases the extrapolated value is presented in addition to the first node value. The total and local energy methods were also used where appropriate.

General description of models

The models analyzed in this paper consist of bi-material plates having cracks in the region of the bi-material interface. These plates are taken as micro-mechanical models of an interfacial region in a composite material containing a flaw or crack. The relationship of the micromodel to the composite region is indicated in Figure 4(a).

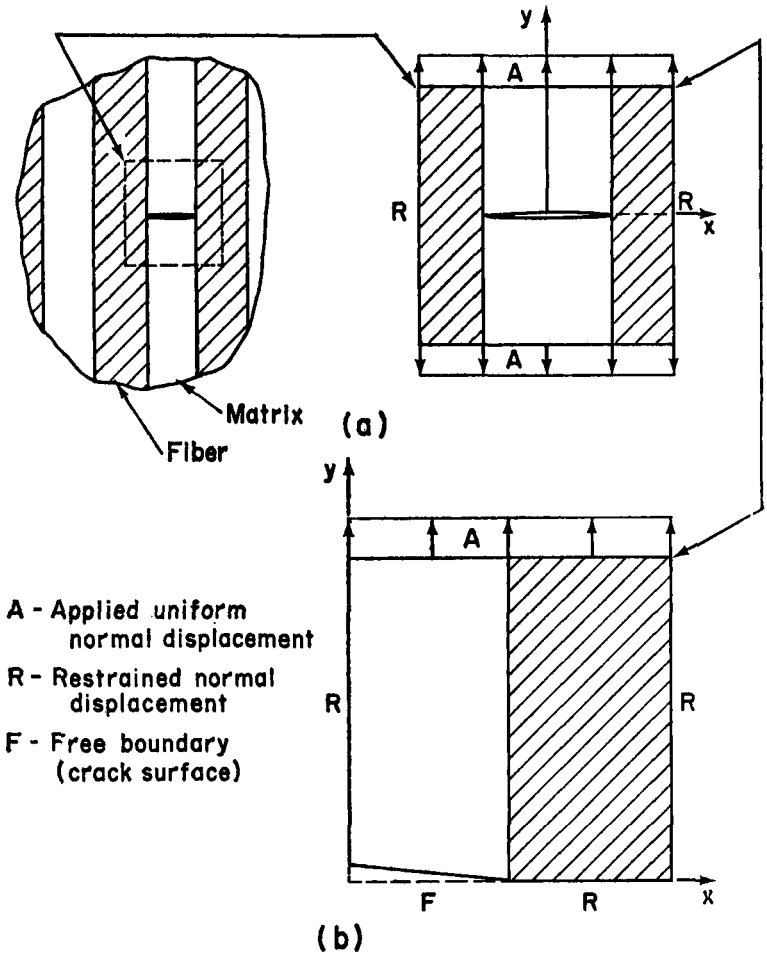

FIGURE 4a Relationship of the micromodel to the composite material.
FIGURE 4b Symmetrical quarter-section analyzed.

The boundary conditions applied to the model are uniform vertical displacements of the upper and lower edges and a zero horizontal displacement of the sides. Due to symmetry about both the centerlines of the model only a symmetrical quarter section of the model was analyzed. A typical quarter section with appropriate boundary conditions is shown in Figure 4(b). The finite element net used for Model II is typical and is shown in Figure 5. In this figure the rollers symbolize a boundary having normal displacements restrained and the arrows along the upper boundary indicate a uniform applied displacement.

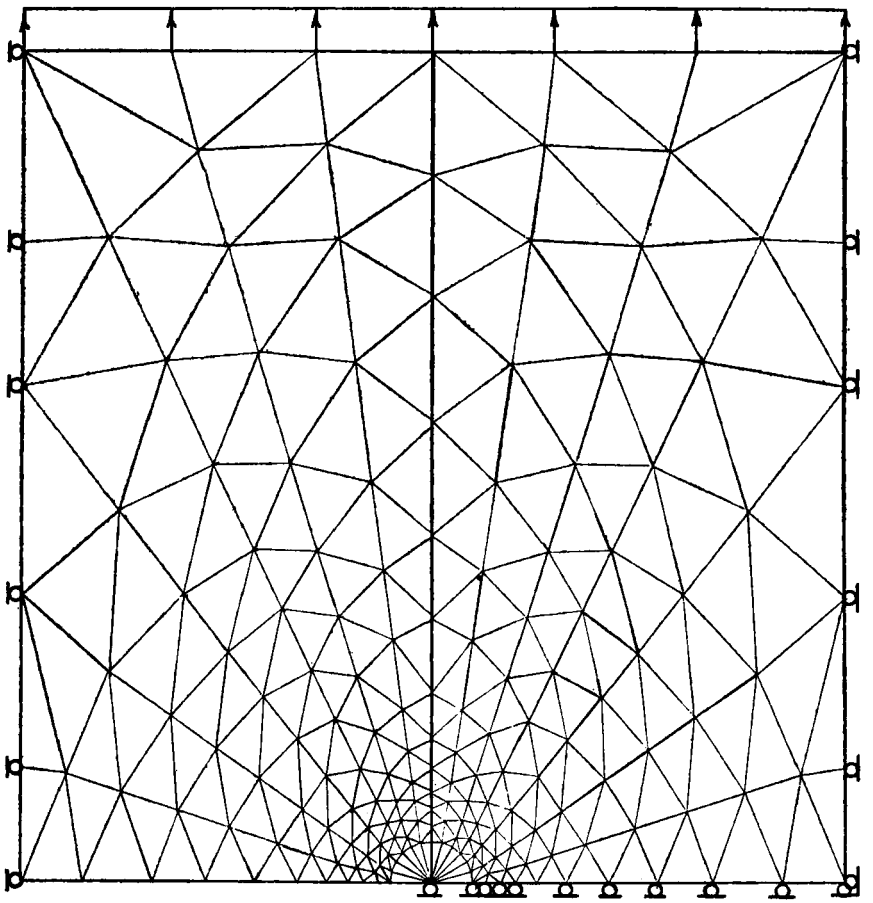

FIGURE 5 Finite element net, Model II.

Five modes of crack progression through the interfacial region were modeled:

I. Crack approaching the interface.
II. Crack tip on the interface.
III. Crack progression along the interface (splitting).
IV. Crack progression through the interface.
V. Crack progression along and through the interface.

Schematic drawings of the five quarter-section models are shown in Figure 6. The displacements of the crack surfaces have been exaggerated in these drawings for clarity. These models are subsequently referred to by these Roman numerals as Model I, Model II, etc.

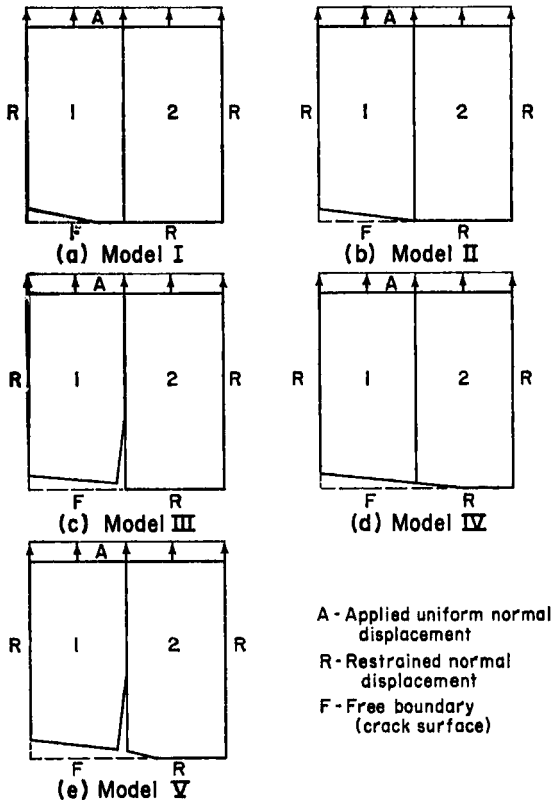

FIGURE 6 Schematic drawings showing the position of the crack in the five model analyzed and nomenclature.

Model verification

Two initial runs were made with each model to verify the input data and the calculation of the fracture parameters. As an initial verification, the nodes along the entire crack face were fixed. This model represents a uniformly stressed tensile specimen and the element stresses can be compared to known values.

After completing the first verification, the crack was modeled by releasing the constraints on the crack face nodes and the material properties in both sides of the model were equal. The analytical solution for K_I for an infinite homogeneous plate containing a regular array of colinear cracks and subjected to uniform tension at infinity is given as

$$K_I = \sigma_\infty \sqrt{2b} \sqrt{\operatorname{Tan} \frac{\pi a}{2b}} \tag{4}$$

where σ_∞ is the tensile stress at infinity, a is the half-crack length and b is the spacing of the cracks.[17]

Although exact agreement cannot be expected due to the finite height of the models, the finite element solutions were compared to the infinite plate solution of (4). The stress intensity factor K_I was computed using the J-integral, $K_I(J)$, the local energy, $K_I(LE)$, the displacement of the first node of the SST element, $K_I(SST)$ and the extrapolated value at $r = 0$, $K_I(EXT)$. These results are shown in Table I for the three models having horizontal cracks. Comparison of the values in Table I shows that most of the calculated

TABLE I
Comparison of stress intensity factors from the finite element solution to the analytically determined value.

Model	Equation (9)	Finite Element Solution			
	K_I^*	K_I (SST)	K_I (EXT)	K_I (J)	K_I (LE)
I	3750	4185	4020	3679	4872
II	3780	3660	4000	3710	4110
IV	3750	3686	4010	3665	4150

• All stress intensity factors have units of psi $\sqrt{\text{in.}}$

stress intensity factors agreed with the infinite plate solution to within about 10 percent. It is judged that the extrapolated values are the best values even though they depart from the infinite plate solution by the widest margin.

Dimensions and definitions

The dimensions of the models, the coordinate system and transverse crack length are defined in Figure 7(a). The bi-material interface divides the body, the material on the left side of the interface is referred to as Material 1 and the material on the right as 2. Material properties or stresses associated with material 1 are denoted by the superscript $^{(1)}$; $E^{(1)}$, $\sigma^{(1)}$, etc.

In all cases the models were loaded with a uniform displacement of 0.01486 inches along the upper boundary. For the homogeneous uncracked tensile models with $E^{(1)} = E^{(2)} = 10^6$ psi and $\nu^{(1)} = \nu^{(2)} = 0.3$ this displacement produced the uniform stresses $\sigma_y = 1000$ psi, $\sigma_x = 428.67$ psi and $\sigma_{xy} = 0$ psi. This displacement was effected using an approximate method described by Zienkiewicz.[30] The uniform displacement boundary loading was chosen for

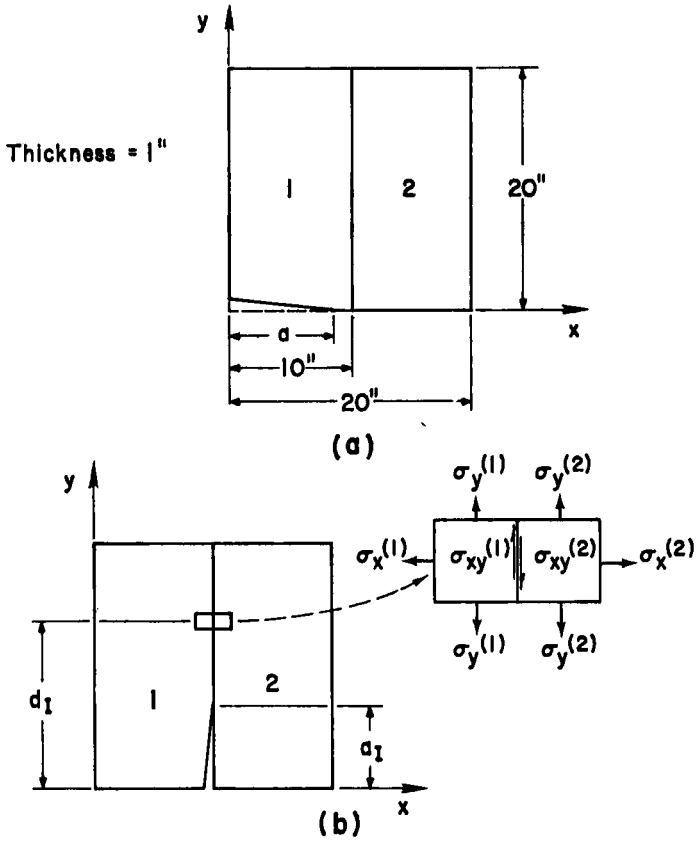

FIGURE 7a Model dimensions.
FIGURE 7b Definition of interfacila crack length and the interfacila stress components.

these tests so that displacements and hence fracture parameters computed from the displacements could be compared from model to model.

Along the interface there are four independent components of stress: σ_x, $\sigma_y^{(1)}$, $\sigma_y^{(2)}$ and σ_{xy} where the superscripts refer to materials 1 and 2. The stresses $\sigma_x^{(1)} = \sigma_x^{(2)}$ and $\sigma_{xy}^{(1)} = \sigma_{xy}^{(2)}$ due to equilibrium along the interface. These stresses are defined along with their location d_I in Figure 7(b). In models having an interfacial crack, the crack length is referred to as a_I as defined in Figure 7(b).

The effect of modulus ratio R, where $R = E^{(1)}/E^{(2)}$, on the stress intensity factor was evaluated by assigning to R the spectrum of values 1/20, 1/10, 1/5, 1, 2, 5, 10 and 20. Unless otherwise noted the Young's modulus of material 2 was kept constant at 10^6 psi and Poisson's ratios for both 1 and 2 were kept constant at 0.3. In the original work[43] the stress distributions along the interface were also presented. These results have some implications concerning interfacial fracture but were judged too voluminous for the present paper.

Model I

Model I contains a horizontal crack, $a = 9$ inches, which resides in material 1, Figure 5(a). The crack tip is one inch from the bi-material interface.

The stress intensity factors were determined for the spectrum of modulus ratios $1/20 \leq R \leq 20$ and are shown in Figure 8. These stress intensity factors were calculated using the displacement of the SST element, the extrapolation method and the local energy method as previously discussed.

These data are well represented by the straight line shown in Figure 8. The equation of this line is $K_I = 4020R$. This variation in stress intensity factor for the bi-material plate is thus of the same form as the variation in K_I with modulus for a homogeneous plate subjected to uniform boundary displacement. It can be inferred from this similarity that the crack tip is sufficiently far from the interface for the square root singularity to be valid.

Comparison of the four interfacial stresses showed that $\sigma_y^{(1)}$ is the largest stress, particularly for large R, and that both $\sigma_y^{(1)}$ and σ_{xy} show severe gradients approaching the crack region. The values of σ_x were much lower and more uniform. Probable modes of interfacial fracture would be crazing normal to the interface due to the high $\sigma_y^{(1)}$ and mode II crack propagation close to the crack region due to the steep gradients of σ_{xy}. Since the values of σ_x were relatively smaller the tendency toward mode I interfacial crack propagation would be small. Due to the direction of the maximum principal stress the crack might tend to curve up above the horizontal plane and intercept the interface at some higher point.

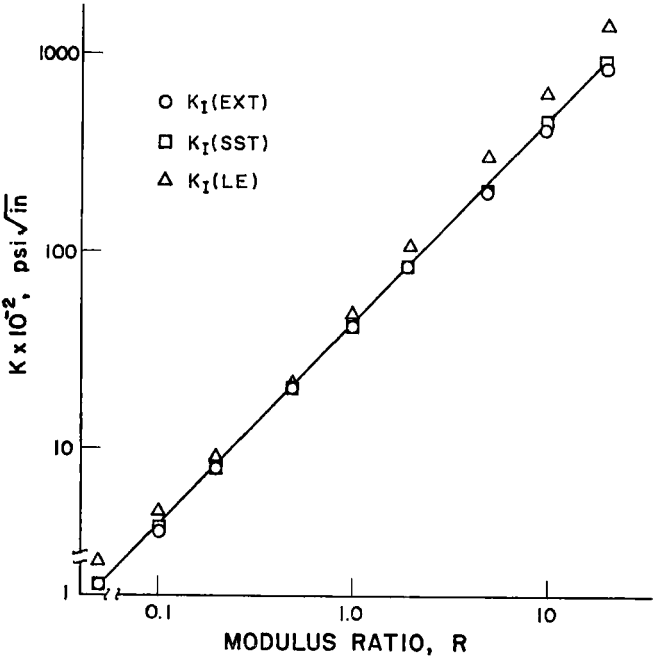

FIGURE 8 Variation of stress intensity factor with modulus ratio, R, for Model I.

Model II

The crack tip in Model II is on the bi-material interface and the crack length, a, is 10 inches, Figure 5(b).

A stress intensity factor is not defined if the singularity departs from $\sqrt{r}$. However, some idea of the "severity" of the crack can be gained by inspecting the profiles of the free surface of the crack for the spectrum of R. These profiles are shown in terms of the crack tip coordinate r in Figure 9. It can be seen that when the modulus of material 1 containing the crack is increased the displacements of the crack surface near the tip increase and the average slopes of the near tip profiles increase. If profiles like these were determined for a homogeneous material, these increased displacements would be interpreted as proportional to increases in the stress intensity factor. It would seem physically plausible to suppose that since the crack is opened more as R increases, the severity of the crack or the tendency of the crack to propagate will be increased.

The main features of the stress distributions were very large values of $\sigma_y^{(1)}$ and σ_{xy} along the interface near the crack tip for large R. The gradients

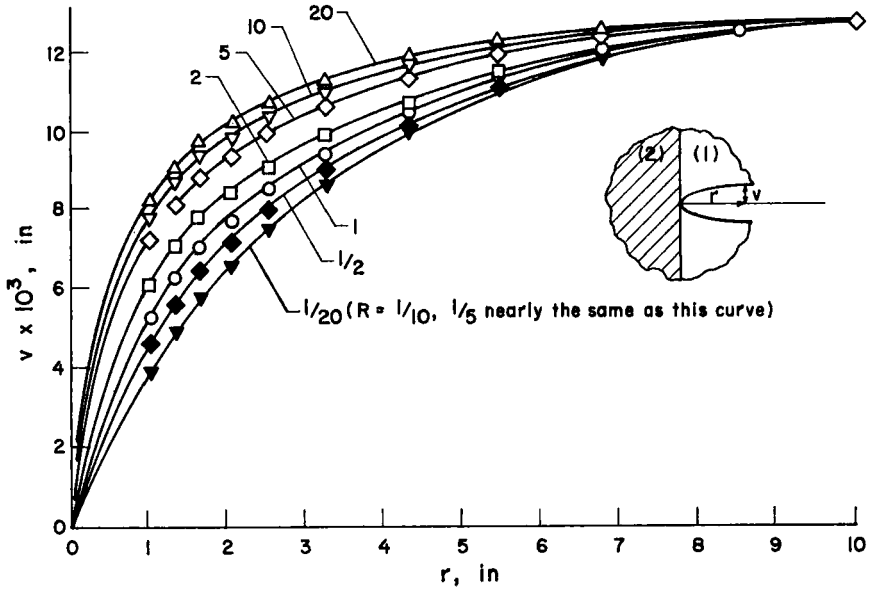

FIGURE 9 Crack surface profiles, Model II, for various modulus ratios R.

of the stresses near the crack tip increase markedly for high values of R indicating the increased severity of the singularity. Generally the stress concentrations for $\sigma_y^{(1)}$, $\sigma_y^{(2)}$, and σ_{xy} were evident near the crack tip. The values of σ_x, though generally lower, were effected at larger distances along the interface which could cause splitting of the crack.

The analyses of Williams[19] and Swenson[28] showed that if the crack tip is on a bi-material interface the singularity will not be proportional to $r^{1/2}$ but will be proportional to r^{λ} where λ is an eigen parameter and depends on the material properties. It was found that the dependence of λ on material properties given by Swenson[28] corresponded within limits to the results of the finite element analysis of Model II. A more complete discussion of this dependence is given in the complete work.[43]

Model III

An analysis was made of the strain energy release rate associated with the propagation of a crack along the bi-material interface. The initial configuration was a model of a horizontal crack, $a = 10$ inches, with the crack tip on the interface. A crack of varying length, a_I, extending up the interface was then modeled, Figure 5(c).

A total of six interfacial nodes were released in sequence to model an

interfacial crack initially of zero length and reaching a maximum length of $a_I = 4.8$ inches. For each crack length the external work applied to the model was computed by numerically integrating the stress across the displaced upper boundary. For an elastic body the change in internal energy is equal to the external work. Thus a curve of work versus crack length can be constructed from the seven finite element solutions and this curve differentiated to determine $\partial U/\partial a$ and hence G.

An energy analysis was made for two material combinations; glass-resin and resin-glass. The modulus ratio of the glass/resin was taken as 20 and the Poisson's ratios for the glass and resin were taken as 0.2 and 0.35, respectively. A uniform boundary displacement of 0.01468 inch was applied to the upper boundary as in the previous models.

The curve of internal energy versus crack length in the one inch thick plate for the glass-resin combination is shown in Figure 10 and for the resin-glass

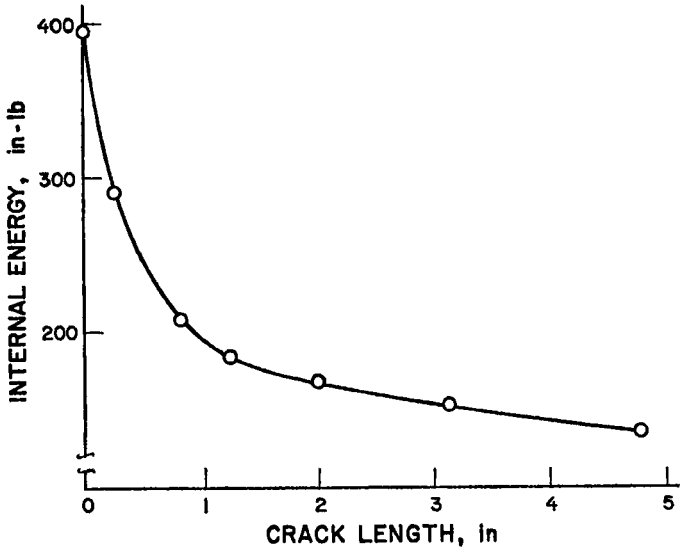

FIGURE 10 The change in internal energy for fixed boundary displacement and varying interfacial crack length, a_I, for glass-resin material combination.

combination is shown in Figure 11. Note that the energy changes for the resin-glass model were very small. These curves were differentiated graphically at each value of crack length to determine G.

The curves of G versus crack length are shown in Figures 12 and 13 for the glass-resin and the resin-glass combinations respectively. Due to the fixed displacement boundary conditions the value of G decreases with increasing crack length in both cases with the glass-resin combination showing the largest decrease.

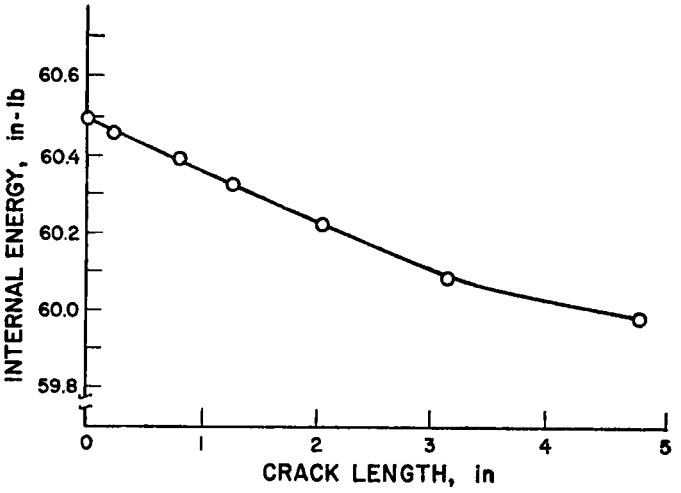

FIGURE 11 The change in internal energy for fixed boundary displacement and varying interfacial crack length, a_I, for resin-glass material combination.

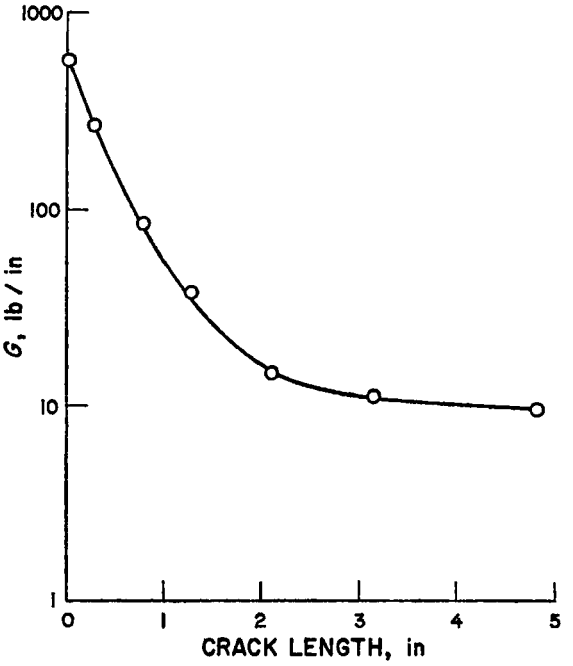

FIGURE 12 Variation in mixed mode crack extension force, G, with interfacial crack length, glass-resin combination.

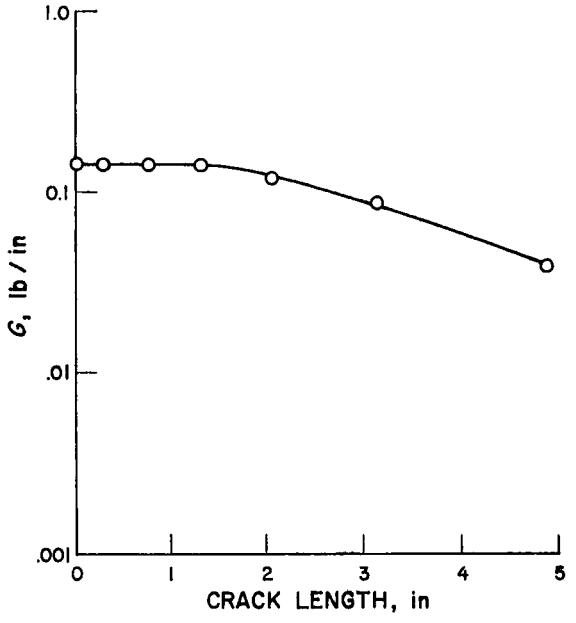

FIGURE 13 Variation of mixed mode crack extension force, G, with interfacial crack length, resin-glass combination.

The applied boundary conditions produce both opening mode (I) and sliding mode (II) displacements of the interfacial crack. The value of G determined from the total energy analysis is made up of the sum of the opening mode component G_I and the sliding mode component G_{II}. The individual values of G_I and G_{II} cannot be directly determined from the total energy analysis.

The displacements of the crack surface may be used with the extrapolation method to estimate the mode I and mode II stress intensity factors K_I and K_{II}.[35] In the case of this model these estimates are only approximate due to the very coarse element net in this region. For an interfacial crack 4.8 inches long, K_I and K_{II} determined from the displacements were the same order of magnitude. For shorter cracks the stress intensity factor K_{II} associated with the shear mode was larger than K_I. This comparison was not made for cracks shorter than 2.02 inches due to the coarse element net.

The relative values of K_I and K_{II} can be put into terms of G_I and G_{II}. Taking these values a curve of G_I/G_{II} versus crack length can be constructed, Figure 14, to qualitatively indicate the effect of this fracture mode transition of the relative values of G_I and G_{II}. The application of these results to composite fracture are discussed in detail in a later section.

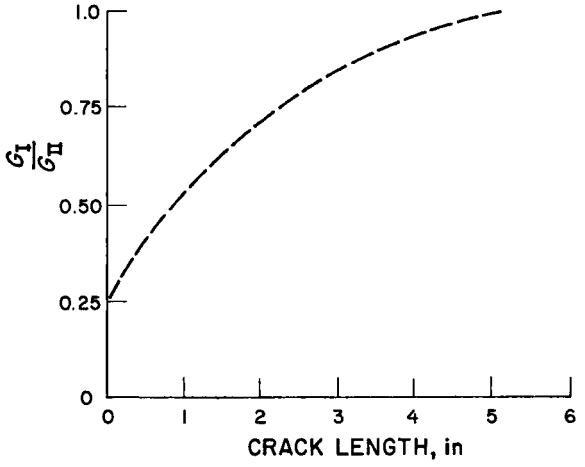

FIGURE 14 Estimated effect of the fracture mode transition on the relative values of G_I and G_{II}.

Model IV

Model IV, Figure 5(d), contains a crack 11 inches long which extends entirely through material 1, penetrates the interface and extends one inch into material 2. Since the crack tip is completely enclosed in material 2 it was assumed to have a square root singularity. The stress intensity factors were computed from the displacements of the first node of the SST element. Since the remainder of the crack surface was in material 1 the extrapolation method did not apply.

The stress intensity factors were computed for the spectrum of moduli $1/20 \leq R \leq 20$ using the displacement of the SST element and the local energy. These values are shown in Figure 15. The differences between $K_I(SST)$ and $K_I(LE)$ are larger than in the other models for extreme values of R. The calculation of $K_I(LE)$ involves squaring the local stresses. Since these elements are large and near the material discontinuity any discrepancy in the finite element approximation to the stresses is amplified. The values of $K_I(SST)$ are probably the more accurate and values of $K_I(EL)$ are included here only for qualitative comparison.

A straight line, $K_I = 3686.0\, R^{0.4}$, has been drawn tangent to the data in the region of $R = 1$. Compared to Model I, Figure 8, these stress intensity factors are seen to be much less sensitive to changes in R and depart slightly from a linear relationship. This behavior would be expected due to the boundary conditions and to the manner in which the moduli were varied.

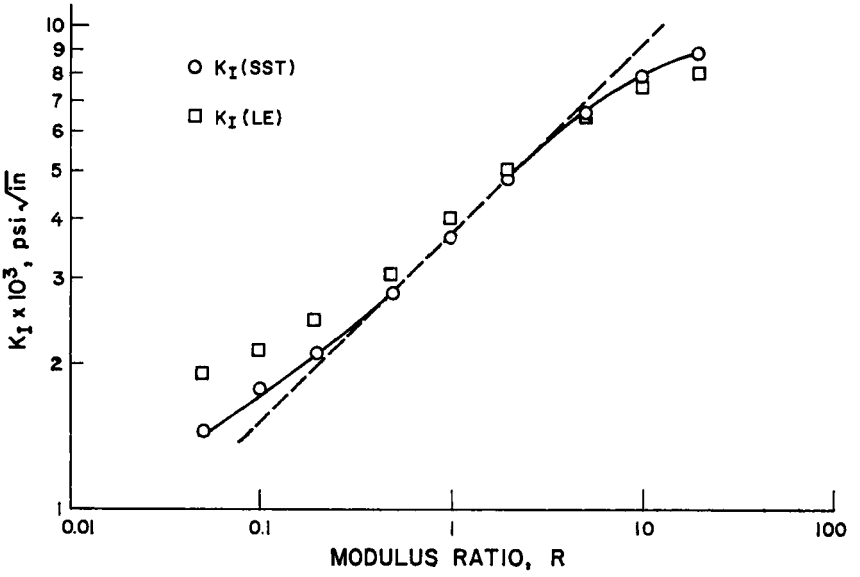

FIGURE 15 Variation of stress intensity factor with modulus ratio, Model IV.

Although the values of $\sigma_y^{(1)}$ and $\sigma_y^{(2)}$ are zero at the free surface of the crack the finite element analysis showed some stress concentrations along the interface near the crack face as R increases. These stress concentrations are due to the discontinuity in material properties. Although $\sigma_y^{(1)}$ and $\sigma_y^{(2)}$ were generally smaller than Models I and II, σ_x was relatively larger for large R indicating that there is a splitting force as the crack emerges from the stiffer phase.

Model V

Model V contains a primary crack which extends through material 1 and one inch into material 2 in a manner identical to Model IV. In addition to this primary crack, Model V has a secondary crack which extends along the interface, Figure 5(e). The purpose of this model was to study the interactions of the primary and secondary cracks.

Two interfacial crack lengths were modeled: $a_I = 1.25$ inches and $a_I = 4.8$ inches. For each of these crack lengths the modulus ratio, R, was set to 1/20, 1 and 20 and the stress intensity factors of the primary crack were determined using the displacement of the SST element.

The results for the two crack lengths are shown in Table II. For comparison Table II also includes the stress intensity factors for the case of no interfacial crack determined from Model IV. The stress intensity factors of the primary

TABLE II
Stress intensity factors, Model V.

Interfacial Crack Length	Modulus Ratio, R	K_I (psi $\sqrt{in.}$)
(no crack)	1/20	1751
	1	3690
	20	8964
a_I = 1.25 in.	1/20	2366
	1	4189
	20	9173
a_I = 4.8 in.	1/20	4459
	1	6515
	20	9718

crack increase as the interfacial crack length increases. This increase is proportionally larger for large R.

This behavior forms the basis for a two-step crack propagation sequence. Assume for example that there is a flaw in material 2 represented by the primary crack but that the stress intensity factor is less than the critical value. If there is a flaw in the interface or if the interface bond is weak a secondary crack may progress along the interface while the primary crack remains stationary. The results from Model V indicate that as this secondary crack progresses the stress intensity factor of the primary crack is increased and hence after some interfacial crack extension the primary crack would extend. This two-step process is observed in composite fracture. These interactions are discussed in greater detail in the next section for the glass and resin material combinations.

The microfracture game

If the fracture toughness values G_c of phase (1), phase (2), and the interfacial bond between (1) and (2) are known for some particular composite then one

has the informaton to play a microfracture game. The five models are analyzed for this material combination and the stress intensity factors or the crack extension force G is determined. By comparing G for the various modes to the appropriate G_c one has a basis for predicting or deciding which mode is most probable. A sample microfracture game for the particular material combinations of glass and resin are given below.

Critical values, G_c

Typical values of the critical crack extension force G_c, for glass, resin and the interface were taken from the literature. These values are shown in Table III along with normalized values $\bar{G}_c$ and $\underline{G}_c$ obtained by dividing the values for the critical crack extension force by the critical crack extension forces for glass and resin, respectively.

The critical values for resin have been determined using cracked-plate models and the interfacial toughness for opening mode displacement G_{Ic} has been determined using a double cantilever beam specimen.[7]

The author is not aware of any interfacial fracture toughness data for shear mode II. Values of G_{IIc} are usually much greater than the value of G_{Ic} for a given material. Fracture data given in Ref. 4 for unidirectional glass-resin laminates suggest that G_{IIc} may be on the order of 10X G_{Ic}. This value was taken as a plausible estimate of G_{IIc} for the interface and is shown with the other data in Table III.

Critical values for glass are given by several investigators. Griffith[15] found a value of 0.00624 lb/in., Shand relates values between 0.0065 and 0.0150 lb/in. for different types of glass, Irwin[17] gives values between 0.04 and 0.08 lb/in. for lantern slide glass and Lowrie[45] presents a value for the surface energy for E-glass which corresponds to a fracture toughness of 0.00456 lb/in. For the purposes of this discussion a nominal value of G_c of 0.006 lb/in. was used, Table III.

The Griffith[15] equation relating tensile strength and crack size is given as

$$\sigma_f = \sqrt{\frac{2E\gamma}{\pi c}} \tag{5}$$

also

$$G_c = \frac{2\gamma}{(1 - \nu^2)} \quad \text{for plane strain} \tag{6}$$

where σ_f is the tensile stress at failure, γ is the surface energy and c is the crack depth. Shand tested glass rods $\frac{1}{4}$ inch in diameter having surface cracks approximately 0.001 to 0.010 inch deep and his results agreed closely with the Griffith relationship, (5). Experiments by Shand, Anderson[46] and others

TABLE III
Critical values, G_c (lb/in.)

Mode I

Material	Nominal Value	Normalized to	
		Glass	Resin
	G_{Ic}	$\bar{G}_{Ic}$	$\underline{G}_{Ic}$
Glass	0.0006	1.0	0.00107
Resin	5.6	935	1.0
Interface	1.0	167	0.179

Mode II

	G_{IIc}	$\bar{G}_{IIc}$	$\underline{G}_{IIc}$
Interface	10.0	1670	1.79

have clearly demonstrated the strong dependence of failure stress on surface condition.

The strengths of very thin glass fibers have been measured for a variety of surface conditions and treatments. The glass fibers used in glass-resin composite fabrication typically have diameters in the range of 0.0002 to 0.0008 inch. The strengths of these thin fibers are sensitive to surface treatment. It is supposed that reductions in strength are related to sub-microscopic flaws in the fabrication of the fibers or caused by the handling or chemical attack of the surfaces.

If one assumes that the failure of these thin fibers is described by the Griffith relationship a value for γ determined directly from the surface energy can be used along with the measured stress at failure to infer the crack size. Considering a filament of E glass having a strength of 500,000 psi, (5) predicts a flaw length of only 14Å.[46] This corresponds to a flaw length/diameter ratio of approximately 10^{-4}. Since a flaw of this size is sub-microscopic its existence is only inferred[47].

Model values, G and K

G and K for Models I through V were determined for the particular material combinations of resin-glass and glass-resin. A glass/resin Young's modulus ratio of 20 was used and the Poisson's ratios of the glass and resin were taken as 0.2 and 0.35 respectively. For the first comparison the material constants

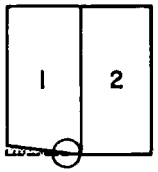

I

$K^{(1)}$	$G^{(1)}$	$G^{(2)}$	$G_c^{(2)}$
209	0.767	1.0	1.0

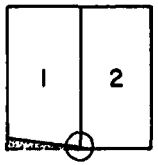

II

(2441)	(104.8)	(137.0)	(1.0)

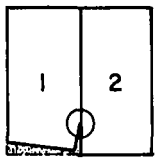

III

(NA)	.141 (3)	0.184 (3)	0.179 (4)
			1.79 (5)

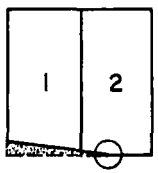

IV

1463	2.05	2.67	0.00107

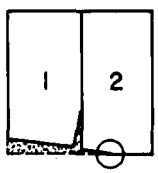

V

2074	4.13	5.4	0.00107

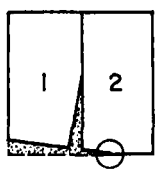

VI

4174	16.75	21.9	0.00107

1 - Resin
2 - Glass

(NA) not available
(1) values for the crack tip in circle ○
(2) normalized to the value for resin.
(3) decreases as the crack proceeds along interface, see Figure 14.
(4) Mode I
(5) Mode II

FIGURE 16 Fracture parameters associated with the various modes of crack propagation in the region of a resin-glass interface.

for resin were assigned to the left side of the model and the material constants for glass were assigned to the right side.

Figure 16 contains schematic diagrams of the models indicating the position of the crack in each model along with the associated fracture parameters determined from the finite element solution for that model. Model V is shown for the two cases of a short interfacial crack (1.25 inches) and a long interfacial crack (4.8 inches).

The first column in Figure 16 shows the stress intensity factors as determined from the displacements of the SST elements. As discussed previously the stress intensity factors are not defined if the crack tip is on the interface, Model II. The numbers shown in the parentheses beside this model were computed using the displacement of the SST element and the material properties of material 1. If the crack tip were enclosed in material 1 as in the case of Model I this number would *be* a stress intensity factor. Since the crack tip is actually on the interface this number is not a stress intensity factor but since it is directly proportional to the opening displacement of the crack surface this number can be compared to the stress intensity factor for Model I to determine the relative magnitude of the crack surface displacements. The severity of this normal interfacial crack is proportional to these displacements although the functional form of this relationship is not defined.

For the case of interfacial fracture, Model III, a total energy analysis resulted in values of G for the mixed mode displacement. Stress intensity factors were not determined. The value of G shown in Figure 16 with Model III is a maximum value and corresponds to G for the initial increment of crack extension along the interface. The value of G decreased with crack length as shown in Figures 12 and 13. The stress intensity factors for all the other models were converted to G's using (3). This was done to allow comparison of the other models to Model III for which only G is known.

In the third column of Figure 16, all the values of G have been normalized to the value of G for Model I where the crack tip is in the resin and is approaching the glass. In column four are shown the critical values G_c, Table III, which have likewise been normalized to the critical value for the resin. Normalizing the values in this manner facilitates the discussion of the alternative modes of crack progression as the crack approaches the interface.

Crack propagation in the resin-glass model

Columns 3 and 4 of Figure 16 contain the normalized values of crack extension force for the model along with the normalized critical values. For Model I the crack is in the resin and approaching the resin-glass interface. The values have been normalized to this model and hence $\underline{G} = \underline{G}_c$ and, by definition, the crack is propagating.

The "stress intensity" for Model II is much higher than Model I for the same external displacement. Although this stress intensity factor for Model II is somewhat fictitious (as discussed previously) it is clear that the stress intensity factor will tend to increase and the crack will tend to propagate from the position shown in Model I toward the interface with no increase in external load. With the crack tip at the interface the next two modes of propagation are along the interface, Model III, or through the interface and into the glass, Model IV.

Model IV represents a crack which penetrates the glass to a depth equal to 0.1 the width of the glass portion of the model. Since the glass portion of the model is a symmetrical half of a two-dimensional glass fiber (Figure 4) the crack depth or flaw depth is $0.05D$, where D is the diameter of the fiber. Comparing columns 3 and 4 in Figure 16 for Model IV clearly shows that if there is a flaw in the glass fiber of $0.05D$, $\underline{G} \gg \underline{G}_c$ and the crack will propagate into the glass with no increase in external load.

Data given in Ref. 46 indicates that a typical flaw in an actual glass fiber used for composite fabrication would be on the order of $0.01D$. In terms of Model IV, if such a typical fiber were modeled and if the critical flaw was located at the point where the resin crack intercepted the interface, the crack length would be only 0.005 times its width instead of 0.1 times the width as shown. If it is assumed that the stress intensity factor for Model IV depends on the square root of the crack length of the normalized value, G for this small flaw would be 0.134 lb/in. This value is still greater than the normalized critical value for glass and the crack would therefore still tend to propagate through the glass.

The likelihood of the resin crack intercepting the glass at the exact location of a critical flaw is small. Assuming that the crack intercepts the interface at a point where the glass is free of large critical flaws an alternate mode of crack propagation would be along the interface as represented by Model III.

Assuming that the mixed mode crack extension force is divided into G_I and G_{II} according to the proportions given in Figure 14 the values of $\underline{G}_I = 0.0037$ lb/in. and $\underline{G}_{II} = 0.147$ lb/in. are established. Comparison of these normalized values with the normalized critical values shows that G_I is the controlling factor. Since the values of G are related to the square root of the boundary displacements, if the boundary displacements are increased by approximately 2.2 times the initial displacement a crack will propagate along the interface. As the crack propagates G changes with crack length as shown in Figure 13. An important feature of this curve is the fact that G does not decrease very rapidly for the first few inches of crack progression. The resistance to crack extension however becomes smaller due to the continual transition from Mode II to Mode I, Figure 14. Thus once the interfacial crack is initiated, it will tend to propagate unstably along the interface. Using

Figures 13 and 14 it is possible to solve for an equilibrium crack length of approximately 4.2 inches.

Looking again at the glass there are three important effects accompanying the interfacial fracture that increase the probability of crack extension into the glass. The first is the immediate fact that the boundary loads were increased by a factor of 2.2 to initiate the interfacial fracture. This increases K by a factor of 2.2 and G by a factor of 4.9 for Model IV which reduces the critical flaw size for fracture of the glass and hence increases the probability of fracture.

A second effect of interfacial fracture is illustrated in Model V. If there is a flaw in the glass ahead of the resin crack (Model IV), as the secondary crack proceeds along the interface the stress intensity factor associated with the flaw in the glass increases. In Figure 16 the value of G for Model IV (no interfacial crack) is 2.64 lb/in. For the short interfacial crack (Model V) G is 5.4 lb/in. and for the long interfacial crack G is further increased to 21.9 lb/in. Due to this effect a flaw which was initially stable in the glass might tend to propagate after the interface had fractured.

A third factor is the "size effect." As the crack proceeds along the interface the relative size of the region in the glass subjected to the increasing stress becomes larger. The probability of finding a critical flaw in this larger region is greatly increased and hence the probability of crack progression into the glass is increased.

These models indicate that cracks can propagate by a discreet two-step process, first along the interface and then through the glass while the displacement of the boundary is held constant. Microscopic examinations of unidirectional composites have shown the general pattern of fracture involving crack propagation through the matrix to the interface, propagation along the interface and eventual propagation through the fiber.[48]

Crack propagation in the glass-resin model

The approach and presentation contained in this section parallels the approach used in the previous section. The roles of the glass and resin have been interchanged so that the crack in Model I is now assumed to reside in the glass and is approaching a glass-resin interface. The material properties of glass were assigned to side 1 of the models and the materials properties of resin were assigned to side 2.

As in the previous case the fracture parameters determined from the finite element solution are shown accompanying descriptive sketches of the models showing the crack locations, Figure 17. Values of the crack extension force in the models have all been normalized by the value of G for Model I where

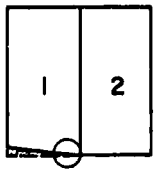

I

$K^{(1)}$	$G^{(1)}$	$\mathcal{G}^{(2)}$	$\mathcal{G}_c^{(2)}$
88,578	7530	1.0	1.0

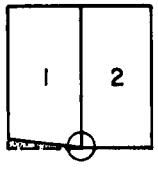

II

(5743)	(31.7)	(0.0042)	(1.0)

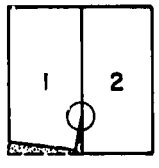

III

(NA)	594 (3)	0.079 (3)	167 (4)
			1670 (5)

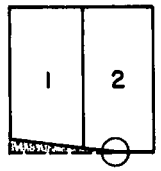

IV

9222	1490	0.198	935

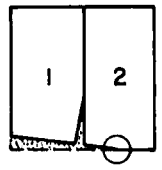

V

9437	1560	0.207	935

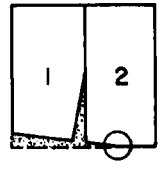

V

10,008	1755	0.234	935

1 - Glass
2 - Resin

(NA) not available
(1) values for the crack tip in circle ○
(2) normalized to the value for glass.
(3) decreases as the crack proceeds along interface, see Figure 14.
(4) Mode I
(5) Mode II

FIGURE 17 Fracture parameters associated with the various modes of crack propagation in the region of a glass-resin interface.

the crack resides in the glass phase. The critical values, G_c, have correspondingly been normalized to G_c for glass, Table III, and are shown in Column 4.

Comparing the normalized values in columns 3 and 4 for Model I, $\bar{G} = \bar{G}_c$ and hence by definition the crack will tend to propagate. Comparison of $\bar{G}$ for Model I and the "$\bar{G}$" for Model II indicates that the severity of the crack decreases as the interface is approached. A total energy analysis between Models I and II for the one inch increment of crack extension yields a value of $\bar{G} = 0.525$ lb/in. which is between the values of $\bar{G}$ for Model I and $\bar{G}$ for Model II and is evidence that the crack extension force drops off as the crack approaches the interface.

It appears that the crack would arrest at some position ahead of the interface for the fixed boundary displacement. If the load were increased by some indefinite amount the crack would progress to the interface. Assuming that the crack does arrive at the interface the two subsequent modes of propagation would either be along the interface or into the resin, Models III or IV.

Assuming as before that for the interfacial failure the mixed mode crack extension force can be divided as shown in Figure 14, the normalized mode I component of G is $\bar{G}_I = 0.0154$ lb/in. The critical value for mode I again controls the initiation of fracture. The ratio of $\bar{G}_{cI}/\bar{G}_I = 10{,}800$ indicating that if the initial displacement on Model I is increased by a factor of $\sqrt{10{,}800}$ or about 104, the crack will tend to extend along the interface. In contrast with the previous resin-glass model, the crack extension force for this model decays rapidly as the crack progresses along the interface, Figure 12. This indicates that for this model there will be no unstable interfacial cracking. In order for the crack to extend, the load on the model must be continually increased above the value for crack initiation.

Considering the case of crack extension into the resin, Model IV, comparison of the crack extension force to the critical value shows that $\bar{G}_{cI}/\bar{G}_I = 9440$. Thus if there is a flaw of the relative size represented in Model IV and if the external displacements are increased by a factor of $\sqrt{9440}$ crabout 97, the crack will propagate into the resin phase.

Comparing Models III and IV it is seen that the tendency for crack extension is about the same for each model. The mode of crack propagation would be controlled by the location and relative size of the flaws. If there was a large flaw in the resin as represented by Model IV and no interfacial flaw the crack would propagate into the resin. If the resin were free of large flaws the crack would slowly propagate along the interface for increasing load. The resin starts to arrest the crack since for either mode of crack progression the external loads would have to be increased by a relatively large amount.

Comparing Model V for the two cases of short and long interfacial cracks

it can be seen that if there is a flaw in the resin the stress intensity factor for this flaw increases as the secondary crack proceeds along the interface. Compared to the resin-glass case for Model V, Figure 16, this increase in the stress intensity factor is small. Thus as the load is increased and as the interfacial crack extends, the strongest factors tending to produce fracture of the resin would be the increased overall load and the size effect discussed previously.

Summary

1) Comparing results from Models I and II for the fixed displacement boundary indicate that if the crack is in the low modulus phase it will tend to propagate unstably to the interface. If the crack is in the high modulus phase it will not propagate to the interface unless the external displacement is increased.

2) The interfacial stresses near the crack face in material 1 always increase with increasing R. The y component and the shear stress are most sensitive to increases in R while the x component changes more gradually.

3) In Model I as the crack approaches the interface $\sigma_y^{(1)}$ and $\sigma_y^{(1)}$ combine to produce a maximum principal stress above the plane of the crack. If the crack propagates normal to the maximum principal stress these results indicate that the crack would branch upward and intercept the interface at an oblique angle. Photomicrographs of normal cracks in a glass-resin composite[48] show that through the glass fiber, $R = 20$, the crack tends to branch upwards as indicated by the analysis.

4) With Model II for $R = 20$ at $d_I = 1$ inch, $\sigma_x = 0.7$ psi, $\sigma_y^{(1)} = 15$ psi and $\sigma_{xy} = 1.8$ psi. These results are in general agreement with the relative interfacial stresses given in the analytical solution by Swenson[28]. For large R, the high values of $\sigma_y^{(1)}$ indicate a tendency toward crazing of phase 1 normal to the interface. For low values of R, $\sigma_y^{(1)}$ is on the same order of magnitude as σ_x which indicates that mode I splitting along the interface becomes more probable. The values of σ_x are also relatively higher at greater distances along the interface as R decreases which would tend to produce longer interfacial cracks.

5) Results from Model III indicated that when the crack is in the low modulus phase, splitting of the crack along the interface is more likely than when the crack is in the stiffer phase.

6) The approximate analysis of the fracture mode transition which is associated with interfacial splitting indicates that this transition may be an important feature of the splitting behavior. Based on these models the fracture mode transition can give rise to an equilibrium interfacial crack length.

7) Results from Models III, IV and V reveal two mechanisms which would cause a two-step, interfacial fracture process consisting of interfacial splitting followed by fiber fracture. The first mechanism is the mode transition discussed above. The second mechanism is the increasing stress intensity factor of the flaw in the fiber as the interfacial crack extends. (The size effect discussed in the text would also contribute to a two-step process.)

Conclusions

1) Recent techniques of finite element fracture analysis can be used to solve microfracture geometries which could not be solved previously.

2) The concepts of linear elastic fracture mechanics when applied to micro models provide a basis of rational discussion of some of the interactions involved in composite fracture.

3) The results of microfracture analysis though highly idealized bear some relation to observed microfracture behaviors and are a necessary step toward rational understanding of the interactions of mechanical and material variables.

Suggestions for continued research

1) Problems of this general type should be analyzed using a more refined grid and/or more sophisticated elements to arrive at improved estimates of the stress intensity factors and stress distributions. The oscillating stresses predicted by some analytical solutions should be compared to refined finite element solutions.

2) In this work it was assumed that the micro model could be simply abstracted from the composite material structure; the boundaries would remain straight and the imposed displacement uniform. In an actual micro region there would be considerable interaction with the surrounding structure and this interaction would change as the crack progressed. It is within the capability of the finite element method to solve this problem.

For example, the "fixed grip" displacement condition imposed on Model III led to the result that the crack progressing along the interface would be arrested. If the boundary condition had been a fixed load the crack extension would undoubtedly have been unstable. In an actual material the boundary condition is somewhere between "fixed grips" and "fixed load" which leads to some equilibrium interfacial crack length. The determination of this crack length would be one of the goals of analyzing an interacting micromodel.

3) The problem of a crack normal to an interface with the crack tip on the interface is complicated and not very well understood. More analytical

work should be done on model geometries which could be built and tested. The main question here is "What is the fracture criterion?" We need some kind of stress intensity factor coupled with experimental determination of critical values for various material combinations.

4) A more detailed examination of the mixed mode nature of interfacial splitting seems warranted since the extent of interfacial splitting or the equilibrium length of an interfacial crack may depend strongly on this mode transition. Thus a fracture analysis may be required in addition to a stress analysis to gain an understanding of the splitting phenomena.

5) With the exponential growth of computing capacity the solution of problems involving large assemblages of micromodels will become feasible. Understanding of the effects of material and structural variables, on for example, cumulative and non-cumulative failure modes might be advanced with the use of these more comprehensive models.

6) Fracture toughness data on a wider range of constituent materials and interfacial combinations in conjunction with improved microfracture analysis would allow one to engage in a broad series of microfracture games. These games would hopefully result in specific recommendations for optimizing composite material toughness and performance.

Acknowledgements

This work was conducted at Vanderbilt University, Nashville, Tennessee. The valuable advice and cooperation of Professors R. Hackett and P. Packman are gratefully acknowledged.

References

1. B. W. Rosen, "Structural Composites—Design and Analysis," *AIAA/ASME 12th Structures, Structural Dynamics and Materials Conference*, Anaheim, Calif., April 1971.
2. E. M. Wu, "Application of Fracture Mechanics to Orthotropic Plates," *TAM Report No. 275*, University of Illinois, 1963.
3. J. R. Hancock and G. D. Swanson, "Toughness of Filamentary Boron/Aluminum Composites", *Composite Materials: Testing and Design*, ASTM STP 497, Philadelphia, Pa. (1972).
4. E. F. Olster and R. C. Jones, "Toughening Mechanisms in Continuous Filament Unidirectionally Reinforced Composites", *Composite Materials: Testing and Design*, ASTM STP 497, Philadelphia, Pa. (1972).
5. A. S. Tetelman, "Fracture Processes in Fiber Composite Materials," *Composite Materials: Testing and Design*, ASTM STP 460, Philadelphia, Pa. (1969).
6. J. R. Hancock, "The Initiation and Growth of Fatigue Cracks in Filament Reinforced Aluminum Alloys," *Composite Materials: Testing and Design*, ASTM STP 497, Philadelphia, Pa. (1972).
7. H. T. Corten, in *Modern Composite Materials*, L. J. Broutman and P. R. Krock, Eds. (Addison-Wesley, New York, 1967). pp. 27–105.
8. Carl Zweben, "Tensile Strength of Fiber-Reinforced Composites, Basic Concepts and Recent Developments," *Composite Materials: Testing and Design*, ASTM STP 460, Philadelphia, Pa. (1969). pp. 528–539.

9. L. J. Broutman, in *Modern Composite Materials*, ed. by L. J. Broutman and P. R. Krock, Eds. (Addison-Wesley, New York, 1967). pp. 337–411.
10. J. O. Outwater, and M. C. Murphy, "On the Fracture Energy of Uni-Directional Laminates," *24th Annual Technical Conference Reinforced Plastics/Composites Division, The Society of the Plastics Industry*, 1969.
11. B. W. Rosen, *Modern Composite Materials*, ed. by L. J. Broutman and J. R. Krock, Eds. (Addison-Wesley, New York, 1967). pp. 106–119.
12. F. J. McGary, in *Fundamental Aspects of Fiber Reinforced Composites*, R.T. Schwartz and H. S. Schwartz, Eds. (Interscience Publishers, New York, 1968). pp. 63–87.
13. C. Zweben, *AIAA Journal* **6** (12), 2325–2331 (1968).
14. J. V. Mullin, J. M. Berry and A. Gatti, *J. Comp. Matrls. II* (1), (1968).
15. A. A. Griffith, *Phil. Trans. Roy. Soc. London*, **Series A (221)**, 163–198 (1920).
16. G. R. Irwin, "Analysis of Stresses and Strains Near the End of a Crack Transversing a Plate," *Trans. ASME, J. Appl. Mech.*, 1957.
17. G. R. Irwin, *Handbuch der Physik* **6**, 551–590 (1958).
18. N. I. Muskhelishvili, *Some Basic Problems on the Mathematical Theory of Elasticity*, 1933; English Translation, P. Noordoff and Company, New York, 1953.
19. M. L. Williams, *Bull. Seismolog. Soc. Am.* **49**, 199–204 (1959).
20. F. Erdogan, *J. Appl. Mech.* **32** (2) *Trans. ASME* **85**, Series E, 232–236 (1963).
21. J. R. Rice and G. C. Sih, "Plane Problems of Cracks in Dissimilar Media," *J. Appl. Mech.* **32** (2) *Trans. ASME* **87**, Series E, 418–423 (1965).
22. G. C. Sih and J. R. Rice, *J. Appl. Mech.* **31**, *Trans. ASME* **86**, Series E, 477–482 (1964).
23. G. C. Sih *et al.*, "Fracture Mechanics Studies of Composite Systems," *Technical Report AFML-TH-70-112, Part II*, Air Force Materials Lab., Wright-Patterson AFB, Ohio, June, 1971.
24. G. C. Sih, P. C. Paris and F. Erdogan, *J. Appl. Mech.* **29**, *Trans. ASME* **84**, Series E, 306–312 (1962).
25. B. M. Maylshev and R. L. Salganik, *Inter. J. Frac. Mech.* **1**, (1965). pp. 114–128.
26. T. T. Wang, T. K. Kwei and H. M. Zupko, *Inter. J. Frac. Mech.* **6**, (2) 127–137 (1970).
27. A. R. Zak and M. L. Williams, *J. Appl. Mech.* **30** (2) *Trans. ASME* **85**, Series E, 142–143 (1963).
28. D. O. Swenson and C. A. Rau, *Inter. J. Frac. Mech.* **6**, 357–365 (1970).
29. R. K. Leverenz, "A Finite Element Stress Analysis of a Crack in Bi-Material Plate," *TAM Report No. 331*, University of Illinois, June, 1970.
30. O. C. Zienkiewicz, *The Finite Element Method in Structural and Continuum Mechanics* (McGraw-Hill, New York, 1967).
31. R. H. Gallagher, "Survey and Evaluation of the Finite Element Method in Fracture Mechanics Analysis," Paper presented at the First International Conference on Structural Mechanics in Reactor Technology, Berlin, W. Germany, September, 1971.
32. G. P. Anderson, V. L. Ruggles and F. S. Stibor, *Inter. J. Frac. Mech.* **7**, (1971). pp. 63–76
33. A. Kobayashi *et al.*, "Application of the Method of Finite Element Analysis to Two-Dimensional Problems in Fracture Mechanics," *Paper 69-WA-PVP-12*, ASME Annual Meeting, November, 1969.
34. J. R. Rice, *Trans. ASME, J. Appl. Mech.* **35**, 379–386 (1968).
35. S. K. Chan, I. S. Tuba and W. K. Wilson, *Engineer. Frac. Mech.* **2**, 1–17 (1970).
36. A. S. Kobayashi, S. T. Chiu and R. Beeuwkes, "Elastic-Plastic State is a Plate with an Extending Crack," *Army Symposium on Solid Mechanics, Light Weight Structures*, AMMRC, 1970.
37. W. K. Wilson, "Crack Tip Finite Elements for Plane Elasticity," *Westinghouse Research Laboratories Scientific Paper 71-1E7-FMPWR-P2, June*, 1971.
38. E. Byskov, *Inter J. Frac. Mech.* **6**, 159–167 (1970).
39. D. M. Tracy, "Finite Elements for Determination of Crack Tip Elastic Stress Intensity Factors," *Technical Report NASA NGL 40-002-080/4 to the National Aeronautics and Space Administration*, Division of Engineering, Brown University, September, 1970.

40. D. M. Tracy, "Finite Elements for Determination of Crack-Tip Elastic Stress Intensity Factors," *AMMRC TR 71-27, Army Materials and Mechanics Research Center*, August, 1971.
41. N. Levy *et al.*, "Small Scale Yielding Near a Crack in Plane Strain—A Finite Element Analysis," *Brown University Division of Engineering, TR NASA NIGL 40-002-080/1*, November, 1969.
42. T. H. H. Pian, P. Tong and C. Luk, "Elastic Crack Analysis by a Finite Element Hybrid Method," *Third Air Force Conference on Matrix Methods in Structural Mechanics*, Dayton, Ohio, October, 1971.
43. C. W. Fowlkes, "A Finite Element Analysis of Cracks in the Region of a Bi-Material Interface," Ph.D. Dissertation, Vanderbilt University, (1972).
44. A. S. Tetelman and A. J. McEvily, *Fracture of Structural Materials* (John Wiley and Sons, Inc., New York, 1967). p. 579.
45. E. Lowrie, *Modern Composite Materials*, L. J. Broutman and P. R. Krock, Eds. (Addison-Wesley, New York, 1967). pp. 270–323.
46. O. L. Anderson, *Fracture*, B. L. Averbach *et al.*, Eds. (John Wiley and Sons, Inc., New York, 1959). pp. 331–353.
47. F. A. McClintock and A. S. Argon, *Mechanical Behavior of Materials* (Addison-Wesley Publishing Co., Inc., Massachusetts, 1966). pp. 488–513.
48. C. A. Bouc,"A Microscopic Study of Mode of Fracture in Filament Wound Glass-Resin Composites," Paper presented at the 19th *Annual Meeting of the Reinforced Plastics Division, The Society of the Plastics Industry, Inc.*, Chicago, Illinois, 1964.
49. L. J. Broutman and S. Sahu, "The Effect of Interfacial Bonding on the Toughness of Glass Filled Polymers," *26th Annual Technical Congress, Reinforced Plastics/Composites Division, The Society of the Plastics Industry*, 1971.